Eur. Phys. J. C 381–395 (2004)
Digital Object Identifier (DOI) 10.1140/epjc/s2004-01960-8

THE EUROPEAN PHYSICAL JOURNAL C

A modified cluster-hadronisation model*

J.-C. Winter[1,a], F. Krauss[1,2,b], G. Soff[1,c]

[1] Institut für Theoretische Physik, TU Dresden, 01062 Dresden, Germany
[2] Theory Division, CERN, 1211 Geneva 23, Switzerland

Received: 12 December 2003 / Revised version: 22 March 2004 /
Published online: 16 July 2004 –

Abstract. A new phenomenological cluster-hadronisation model is presented. Its specific features are the incorporation of soft colour reconnection, a more general treatment of diquarks including their spin and giving rise to clusters with baryonic quantum numbers, and a dynamic separation of the regimes of clusters and hadrons according to their masses and flavours. The distinction between the two regions automatically leads to different cluster decay and transformation modes. Additionally, these aspects require an extension of individual cluster-decay channels that were available in previous versions of such models.

1 Introductory note

Multi-hadron and jet production in high-energy particle reactions is a basic property of the strong interaction [1–3]. A successful description relies on a factorisation, which permits the separation of the perturbative evolution from the non-perturbative development of an event. The perturbative regime can be characterised through calculations of hard matrix elements and subsequent multiple parton emissions – the physically appealing parton-shower picture[1]. The entire hadron-production mechanism, however, cannot be precisely predicted because of the lack of understanding of non-perturbative QCD effects, i.e. hadronisation. For the transition of a coloured partonic system into colourless primary hadrons, this implies, in the context of event generators, a need for phenomenological hadronisation models. Once this primary-hadron genesis has been accomplished, in the last step of the evolution all unstable hadrons decay, so that decay chains of various complexity may appear. Employing the separation ansatz, Monte Carlo QCD event generators such as JETSET/PYTHIA [6,7] or HERWIG [8,9] proved to be a successful tool for the description of multi-particle generation in high-energy physics.

The transformation of the outgoing coloured partons into colour-singlet hadrons reflects the non-perturbative confinement property of QCD. For this transition, the development of phenomenological models may be seen as an attempt to bridge the gap between the theoretically predicted gross features and the experimentally observed detailed event structures. In order to estimate systematic uncertainties in the description of experimental data, which are due to hadronisation, it is important to formulate more than one single unique model. In fact, realistic models can be based upon different concepts and ideas, and their parameters must be extracted from data. Such parameters do not always need to have a clear physical interpretation, since the underlying models by construction are not based on first principles. However, the overall quality of these models can be judged according to whether they reproduce coarse features of the parton–hadron transition or not.

On general grounds, the expectation is that hadronisation effects should give rise to corrections to quantities that are computable in perturbation theory, which are proportional to $1/E^n$, where in the case of e^+e^- event shapes the dominant non-perturbative effects have a $1/E$ dependence on the hard process energy scale E. Hence, a soft hadronisation mechanism, which involves only modest transfers of momentum or quantum numbers between neighbouring regions of phase space, seems to be favoured. Fragmentation models can be studied either in purely analytical terms or in terms of Monte Carlo techniques, which can be implemented in computer programs. The former approach allows predictions to be made without any detailed assumptions concerning hadron formation. On the other hand, the Monte Carlo approach is used to generate the complete conversion exclusively, from the perturbative partonic state to the primary hadrons.

Concerning this intrinsically non-perturbative transition process, different strategies exist and the corresponding Monte Carlo schemes are either based on the Feynman–Field or independent fragmentation model [10], on the Lund string model [11–14] and UCLA model [15] (JETSET/PYTHIA), or on the cluster-hadronisation model (HER-

* Work supported in part by the EC 5th Framework Programme under contract number HPMF-CT-2002-01663.

[a] e-mail: winter@theory.phy.tu-dresden.de
[b] e-mail: krauss@theory.phy.tu-dresden.de
[c] e-mail: Soff@physik.tu-dresden.de

[1] Perturbative QCD cascades can be formulated in two complementary ways, either in terms of quarks and gluons or in terms of colour dipoles [4,5].

WIG). The latter concept[2], initially proposed by Wolfram and Field [18,19], and further advanced, among others [20], by Webber and Marchesini [21–23], explicitly rests upon the preconfinement property of QCD [24] and the LPHD hypothesis [25]. Such cluster models are usually formulated in terms of two phases: cluster formation accomplished through the non-perturbative splitting of gluons left by the parton shower into quark–antiquark pairs, and cluster decays requiring the additional creation of light-flavour pairs. In the $N_C \to \infty$ limit all these quarks and antiquarks can be uniquely formed into colour-singlet clusters, which in their turn mostly undergo simple isotropic decays into pairs of hadrons, chosen according to the density of states with appropriate quantum numbers. Since the parton shower exhibits preconfinement, the mass spectrum of the formed clusters is universal, strongly peaked at low mass and falls off rapidly. But this does not necessarily exclude that clusters of large mass arise after the perturbative phase. Isotropy is not a good approximation for the break-up of massive clusters. Thus, in order to describe the experimental data, one first has to split the high-mass clusters into lower-mass ones employing a longitudinal or string-like mechanism. Then, in this context, one may conclude that cluster-hadronisation models have shown a tendency to evolve in the direction of the string-fragmentation approach.

The exploration of yet uncharted energy domains is the major goal of new enterprises such as the Large Hadron Collider (LHC), which will provide proton–proton collisions at a centre-of-mass energy of 14 TeV. Therefore, our understanding of QCD will play an essential role in analysing and decoding the immense data that will be collected by the detectors of this new experiment. Thus, it is a crucial point that the best possible control on the QCD production and decay mechanism, and the uncertainties related to their description be available. To understand the physics at present and future colliders, e.g. the Tevatron at Fermilab and the LHC at CERN, one fundamental cornerstone is the implementation of new Monte Carlo event generators, e.g. PYTHIA7 [26–28], and HERWIG++ [16, 26, 29, 30]. The development of the Monte Carlo event generator SHERPA (Simulation of High Energy Reactions of PArticles) [26, 31–33] entirely written in the object-oriented programming language C++ is a step in the same direction. With the prospects of LHC physics approaching and Tevatron Run II results coming in, the complexity of simulation programs for hadron colliders has considerably grown. To maintain such complicated programs in a convenient way, the privileged development strategy should be the one that supports a shift towards increased modularity. It is becoming feasible to use one program to produce a hard process, another to evolve the event through a parton shower, and perhaps a third to hadronise the coloured final-state products of the shower. Exactly, on that score, the modified phenomenological cluster-hadronisation model presented in this paper contributes as a further module to the construction of the SHERPA package. The basic features of the new model are the following.

[2] Recent developments may be found, e.g. in [16, 17].

Soft colour reconnection is accounted for in the formation and decay of clusters. The flavour-dependent separation of the cluster regime from the region of hadron resonances yields the selection of specific cluster-transition modes. The two regimes are distinguished by comparing the mass of the cluster with the masses of the accessible hadrons matching the cluster's flavour structure. The method for flavour selection is arranged so that the meson and baryon as well as the strangeness and non-strangeness sector can be influenced separately, and their corresponding ratios can be controlled by a baryon- and a strangeness-suppression parameter, respectively. In addition, the set-up of the probabilities of choosing distinct hadron species supports the approximate maintenance of strong-isospin symmetry at the primary-hadron level.

So far, the cluster scheme presented here is implemented only for electron–positron annihilation, and, for simplicity, only the light-quark sector is considered. An extension to heavy quarks, however, is straightforward.

This paper, describing our cluster-hadronisation model, is organised as follows: first, different aspects of cluster formation are discussed in Sect. 2. Subsequently, in Sect. 3, the parametrisation of light-flavour pair creation is presented. The model's description is concluded by exhibiting cluster transformation and fragmentation processes, which lead to the emergence of primary hadrons; see Sect. 4. The first results obtained with the new hadronisation scheme are shown in Sect. 5 for the process $e^+e^- \to \gamma^*/Z^0 \to d\bar{d}, u\bar{u}, s\bar{s} \to$ hadron jets.

2 Cluster formation

The parton shower describes multiple parton emission in a probabilistic fashion [22, 34, 35]. By factorising the full radiation pattern into individual emissions, it employs the large-N_C limit of QCD. This organises a binary tree, i.e. a planar structure, of the partons. It also ensures that, once the colour structure of the initial partons from the hard matrix element has been fixed, the colour structure of the partons at the end of the parton shower is unambiguously determined.

After the parton shower has terminated, phenomenological hadronisation models set in. To test their impact on corresponding predictions at the hadron level, they should be constructed such that they can be applied independently of the details of the perturbative phase of event generation. Nevertheless, these details matter, since they influence the optimal choice of parameters of the hadronisation model. In the past this led to the simultaneous tuning of perturbative and non-perturbative parameters of various Monte Carlo models [36, 37].

In our model, the non-perturbative transition of coloured partons into primary hadronic matter, clusters, is accomplished by the following steps.

(1) To guarantee the independence of the hadronisation model from the quark masses eventually used in the parton shower and to account for a gluon mass needed by the model, all partons are brought to their constituent masses [21], $\mathcal{O}(0.3\,\mathrm{GeV})$, $\mathcal{O}(0.3\,\mathrm{GeV})$ and $\mathcal{O}(0.45\,\mathrm{GeV})$ for

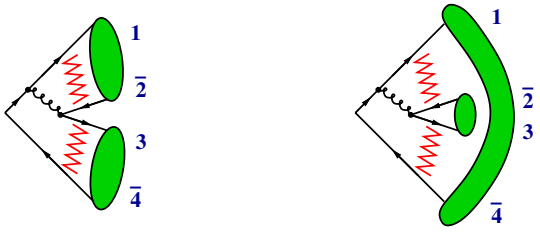

Fig. 1. Both options of cluster formation for a minimal $qg\bar{q} \to q\bar{q}'q'\bar{q}$ cascade. The zig-zag lines connecting the quark lines symbolise the soft exchange of colour quantum numbers, which is responsible for the colour reconnection

u, d and s flavours, and $\mathcal{O}(1\,\mathrm{GeV})$ for the gluon, respectively. For this transition a numerical method, involving several particles and consisting of a series of boosts and scaling transformations, is employed. However, these manipulations are applied only to parton-shower subsets that are in a colour-singlet state.

(2) Since in cluster-hadronisation models the clusters consist of two constituents in a colour-neutral state made up of a triplet–antitriplet, the gluons from the parton shower must split (at least) into quark–antiquark pairs [19]. So, a transition – in principle of non-perturbative origin – $g \to q\bar{q}, \overline{D}D$ into a light quark–antiquark pair $q\bar{q}$ or a light antidiquark–diquark pair $\overline{D}D$ (see Sect. 3) is enforced for each gluon. The respective flavour composition of the gluon's decay products is obtained with the same mechanism as used for cluster decays; see Sect. 3. Quarks or diquarks that cannot be produced owing to too high masses are discarded. The kinematical distribution obeys axial symmetry; the energy fraction z of the quark (antidiquark) with respect to the gluon is given by a density proportional to $z^2+(1-z)^2$, i.e. the gluon splitting function[3]. The limits on z are fixed only after the flavour of the decay products has been selected.

(3) In contrast to the Webber model of cluster fragmentation [38], our hadronisation model may also incorporate soft colour reconnection[4] effects by eventually rearranging the colours of the partons forming the clusters. Starting with a simple cascade, Fig. 1 schematically shows the two options to arrange two colour neutral clusters out of four quarks or diquarks. The first – direct – case corresponds to the usual cluster formation and reflects the leading term in the $1/N_\mathrm{C}$ expansion. The second – crossed – configuration keeps track of subleading terms. Motivated by the well-known colour suppression of non-planar diagrams with respect to planar ones, the relative suppression factor due to the colours is taken to be $1/N_\mathrm{C}^2$.

However, the results from the W mass reconstruction at LEP2 in $e^+e^- \to W^+W^- \to$ jets have indicated that the effects of reconnections are overestimated when the suppression is merely taken to be due to colours. The locality assumption of cluster hadronisation stemming from space-time picture considerations contradicts presumptions, which would enable colour reconnections over a large distance in phase space. Relying on that, a sensible assumption would be that partons close in momentum space are more likely to be colour connected. Therefore, a kinematical weight is additionally applied for each of the two possible cluster pairings. For the pairing ij, kl this weight reads

$$W_{ij,kl} \;=\; \frac{t_0}{t_0 \,+\, (w_{ij}+w_{kl})^2}\,, \tag{1}$$

where the quantity t_0, of the order of $1\,\mathrm{GeV}^2$, denotes the scale where the parton-shower evolution stops and hadronisation sets in. As a measure, w_{ij} functions such as the invariant mass

$$m_{ij} \;=\; \sqrt{(p_i+p_j)^2} \tag{2}$$

of the parton pair (and therefore the cluster), or their relative transverse momentum, similar to the Durham $k_\perp$ jet scheme [44]:

$$p_{\perp ij} \;=\; \sqrt{2\,\min\{E_i^2, E_j^2\}\,(1-\cos\theta_{ij})} \tag{3}$$

might be used. The purely phenomenological ansatz in (1) is in line with the idea employed e.g. in the model of Lönnblad [41] where one minimises the string "length" between colour-connected partners. Here the weight is chosen to be in a simple form ensuring $0 \le W_{ij,kl} \le 1$. It compares the hadron squared-mass scale t_0, i.e. an upper limit for this scale, with the squared sum of the measures for the two pairs. If this value is well below that scale, weights greater than $1/2$ are obtained, which in the case of m_{ij} means that the two pairings have masses of the order of $1/2\sqrt{t_0}$. Otherwise the configurations become more and more kinematically suppressed. In essence, any measure, which can give energy scales of hadronisation for the preferred configurations, is suitable for application.

The actual colour configuration of the considered four-parton set is then chosen according to the combined colour and kinematical weight. For the entire system, ultimately, this reshuffling is iteratively applied to combinations of two colour-singlet pairs of partons in the colour-ordered chain.

Of course, users who are not interested in colour reconnection are given the possibility to entirely switch off this option.

(4) Afterwards the cluster formation is accomplished by merging two colour-connected partons, quark or antidiquark and antiquark or diquark, into a colourless cluster. In this way, four different cluster types may arise, mesonic ($q_1\,\overline{q_2}$ and $\overline{D_1}\,D_2$), baryonic ($q_1\,D_2$), and antibaryonic ($\overline{D_1}\,\overline{q_2}$) clusters. The total four-momentum of these clusters is just given by the sum of their constituent four-momenta [19].

[3] Obviously, for antidiquark–diquark pairs, this is a simplistic assumption, since it neglects, at least, the different spin structure of diquark production.

[4] Other soft colour reconnection models are presented, e.g. in [39, 40]; see also [8, 41–43].

3 Parametrisation of light-flavour pair production

In our model the gluon splitting at the beginning of the cluster formation phase and all cluster decays rely on the emergence of light-flavour pairs [19,21]. During hadronisation, which typically sets in at a scale of 1.0 GeV, there is no possibility for heavy-flavour pair generation [45]. The appearance of baryonic structures is tied to the creation of light diquark–antidiquark pairs[5]. In contrast to the Webber model, in our approach the total diquark spin S is explicitly considered. Thus, $q\bar{q}$ and $\overline{D}_S D_S$, where

$$q \in \{d,\, u,\, s\}$$

and

$$D_S \in \{dd_1,\, ud_0,\, ud_1,\, uu_1,\, sd_0,\, sd_1,\, su_0,\, su_1,\, ss_1\},$$

occur as the possible pairs. Apart from their masses influencing their emergence, the created pair functions only as a flavour label. Furthermore, the pair generation is assumed to factorise, i.e. to be independent of the initial flavour configuration. Therefore, the only interest lies in finding suitable pair-production probabilities, i.e. flavour and spin symmetries should be correctly respected and reasonable hadron multiplicities should be finally obtained in the hadron production.

In our model a phenomenological parametrisation of light-flavour pair production is achieved by employing hypotheses leading to a general "flavour dicing" scheme. This scheme is applied to both regimes, cluster formation and decay. The hypotheses are the following.
(1) The emergence of diquarks, i.e. baryons, is suppressed through a factor $p_{\mathcal{B}}$ with $0 \leq p_{\mathcal{B}} \leq 1$.
(2) $\mathrm{SU}(3)_F$ symmetry is applied, but is assumed to be broken. This is modelled by a strangeness suppression parameter p_s, $0 \leq p_s \leq 1$, whereas the production of d and u flavours is taken to be equally probable (strong-isospin symmetry); hence

$$p_{d,u} \;=\; \frac{1-p_s}{2}\,, \tag{4}$$

and, as mentioned above, $p_{c,b} \equiv 0$.
(3) Spin and flavour weights: the spin-S diquark states ($S = 0, 1$) get a weight proportional to $2\,S{+}1$. Additionally, a combinatorial factor of 2 and 1 is applied, depending on whether different or equal flavours constitute the diquark. But, under the assumption of full $\mathrm{SU}(3)_F$ symmetry, the fact that all states in the baryonic $\mathrm{SU}(3)_F$ octet and $\mathrm{SU}(3)_F$ decuplet appear equally likely has to be reproduced. This gives rise to extra weights on the individual diquark types. In particular, the combined diquark weights w_D^S read (up to the baryon suppression factor):

$$w^{S=0}_{D=ud,sd,su} \;=\; p_D\,, \tag{5}$$

$$w^{S=1}_{D=ud,sd,su} \;=\; 3\cdot p_D\,, \tag{6}$$

$$w^{S=1}_{D=dd,uu,ss} \;=\; 4\cdot p_D\,, \tag{7}$$

where

$$p_D \;=\; \frac{p_{d,u}^{2-n_s}\cdot p_s^{n_s}}{3p_s^2 - 2p_s + 3} \tag{8}$$

and n_s denotes the number of strange quarks in the diquark.

An approach respecting SU(6) flavour-spin symmetry instead is currently investigated.

4 Cluster transitions into primary hadrons

Once the clusters have been formed, their masses are distributed continuously and independently of the hard process with a peak at low mass. In contrast, the observable hadrons have a discrete mass spectrum and, hence, the clusters must be converted. This is achieved through binary cluster decays and through transformations of individual clusters into single primary hadrons. Our model does not incorporate the subsequent decays of unstable hadrons. To model the cluster transitions, the following assumptions are employed.
(1) Cluster fragmentation is universal, i.e. independent of the hard process and of the parton shower. Apart from the collapse of low-mass clusters into one single hadron, clusters disintegrate locally without impact on other clusters.
(2) Cluster transitions, i.e. decays as well as transformations, involve only low momentum transfer, of the order of 1 GeV [21], since hadronisation effects are supposed to be sufficiently soft and hadronisation corrections to parton-level event shapes such as the mean thrust scale inversely with the centre-of-mass energy.
(3) The regime of clusters is separated from the regime of hadrons according to the flavours of the cluster constituents and the accessible hadron masses. Clusters are supposed to be hadrons, if their mass is below a threshold mass. This bound is given by the maximum of the heaviest hadron with identical flavour content and the sum of the masses of the lightest possible hadron pair emerging in the decay of those clusters.

The last assumption has two consequences, namely that in a first step the newly formed clusters that are already in the hadronic regime have to be transformed into hadrons; in the subsequent binary decays of the remaining clusters, that also the daughter clusters, which fall into the regime of hadron resonances, have to become hadrons immediately.

In both cases, a definite hadron species $\mathcal{H}$ has to be chosen according to the flavour structure of the considered cluster $\mathcal{C}$. Respecting fixed particle properties, this choice is based on hadron wave functions motivated by a non-relativistic quark model. The wave functions are factorised into a flavour- and a spin-dependent part. In our model the flavour part is given for a two-component system in terms of quarks and diquarks. The overlap of this flavour part with the flavour content of the cluster gives rise to a flavour weight. In addition, since spin information is washed out in the clusters [21], the total spin J of the hadron manifests

[5] Our treatment of static diquark properties resembles to some extent the one employed in the original Lund approach for baryon production [45].

itself as a corresponding weight. The total spin is given through the coupling of the relative orbital momentum L with the net spin S of the valence components. This can be written as $\mathbf{J} = \mathbf{L} + \mathbf{S}$. The contributions of states with different orbital momentum L to the total-spin sum are accounted for by some a priori weights $\mathcal{P}_L$, which enter as model parameters. Taken together, the total flavour-spin weight $\mathcal{W}$ for a single hadron reads

$$\begin{aligned}\mathcal{W}\big(q_1 s_1, \bar{q}_2 s_2 \to \mathcal{H}^J(q_1 s_1, \bar{q}_2 s_2)\big) \\ \sim \frac{\left|\langle\psi_F(\mathcal{H}^J)|q_1 s_1, \bar{q}_2 s_2\rangle\right|^2}{\sum_{\hat{\mathcal{H}}|\hat{J}=J}\left|\langle\psi_F(\hat{\mathcal{H}}^{\hat{J}})|q_1 s_1, \bar{q}_2 s_2\rangle\right|^2} \\ \times \frac{\sum'_{L,S\to J}\left|\langle S|s_1 s_2\rangle\right|^2 \mathcal{P}_L \left|\langle J|LS\rangle\right|^2}{\sum_{\hat{J}}\sum'_{\hat{L},\hat{S}\to\hat{J}}\left|\langle\hat{S}|s_1 s_2\rangle\right|^2 \mathcal{P}_{\hat{L}} \left|\langle\hat{J}|\hat{L}\hat{S}\rangle\right|^2} . \end{aligned} \tag{9}$$

In contrast to q_1 denoting the quarks, $\bar{q}_2$ stands for antiquarks as well as diquarks. The spins of the two cluster components 1 and 2 are given by $s_1 = s(q_1)$ and $s_2 = s(\bar{q}_2)$, respectively, and $\langle\psi_F(\mathcal{H}^J)|$ denotes the flavour part of the hadron wave function[6]. Moreover, $|\langle j|ls\rangle|^2 = 2j+1/\left(\sum_{i=|l-s|,\ldots,(l+s)} 2i+1\right)$ and $\sum'_{L,S\to J}$ is an abbreviation denoting a summation over $L = 0, 1, \ldots$ and $S = |s_1 - s_2|, \ldots, (s_1 + s_2)$, considering the condition that only those terms contribute, where $|L-S| \le J \le (L+S)$ can be fulfilled. Finally, it should be stressed that the second term of (9) represents only a static model, which accounts for the correct selection of hadrons according to their total spin.

The cluster fragmentation into primary hadrons is performed in two phases.

(I) When the clusters are formed from colour-connected pairs of quarks and diquarks, some of them, because of their comparably low mass, fall into the hadronic regime. Within our framework these clusters are transformed into single hadrons immediately. In doing so, however, some four-momentum is released and has to be absorbed by other clusters. By allowing hadrons with masses lower than the cluster mass only, the momentum transfer is taken to be a mere energy transfer and, therefore, is time-like. This ensures that the absorbing cluster becomes heavier. To fulfill the low momentum-transfer requirement, the already outlined hadron-selection procedure according to the flavour-spin weights $\mathcal{W}$ is modified through the inclusion of an additional – kinematic – weight, which behaves like

$$\mathcal{W}_{\text{kin.}} = \exp\left[-\left(\frac{Q^2}{Q_0^2}\right)^2\right] . \tag{10}$$

In this equation $Q^2 > 0$ denotes the squared momentum (i.e. energy) transfer, and Q_0 is the scale related to the low momentum-transfer demand. The limit Q_0, furthermore, depends on the cluster mass and is also employed in the cluster decays; see below, (12). Note that in the Webber model the clusters being too light to decay are identified to be the lightest hadron with identical flavour structure [38]. In comparison with the Webber scheme, the major difference of our approach in the case of single-cluster transitions is the expansion of the hadron-selection procedure, i.e. the selection is not restricted to the lightest hadron anymore; instead all hadrons with masses lower than the cluster mass are allowed to be selected.

The cluster compensating the residual four-momentum is selected such that it contains the partner that emerged in the same non-perturbative gluon-splitting process as one of the constituents of the transformed cluster. In turn, clusters, which fall into the hadron regime and contain two leading quarks, are always split non-perturbatively into two clusters containing only one leading constituent. In this context leading partons, however, are only those quarks and antiquarks that directly originate from the perturbative phase, and not from the non-perturbative gluon splitting or from the cluster decays. For the resulting single-leading clusters, then, the same considerations as for the direct transformation to hadrons apply. In case a cluster in the hadron regime is made up of a diquark and an antidiquark, which is, in principle, possible, it is forced to specifically decay into two mesons. The kinematics details on both the forced double-leading cluster break-up and the double-diquark cluster decay are the same as outlined below in paragraph (II); see (11).

(II) Finally all remaining clusters – primary clusters as well as secondary clusters (daughters) – have to be split. The mass categorisation outlined above automatically yields one of the modes $\mathcal{C} \to \mathcal{C}_1\mathcal{C}_2$, $\mathcal{C} \to \mathcal{C}_1\mathcal{H}_2$, $\mathcal{C} \to \mathcal{H}_1\mathcal{C}_2$, or $\mathcal{C} \to \mathcal{H}_1\mathcal{H}_2$. These modes involve the creation of an extra flavour pair according to the ideas illustrated in Sect. 3. Similarly to the cluster-formation phase, then, two flavour configurations for the decay products emerge, namely a direct one and a crossed one; see Fig. 2. Again, the crossed configuration is suppressed by the colour factor $1/N_{\text{C}}^2$ and the kinematical weight from (1) using identical measure functions w and replacing t_0 by Q_0^2, which again depends on the mass of the decaying cluster.

Furthermore, the mother-cluster fission kinematics, which makes use of the scale Q_0, is fixed to be anisotropic, and, as already discussed in the introduction, this breaking mechanism is chosen to have string-like characteristics. Starting from a mother cluster with constituent momenta $p_{1,2}^{\mathcal{C}}$ and mass $M_{\mathcal{C}}$, the new momenta of the decay-products' constituents read [21]

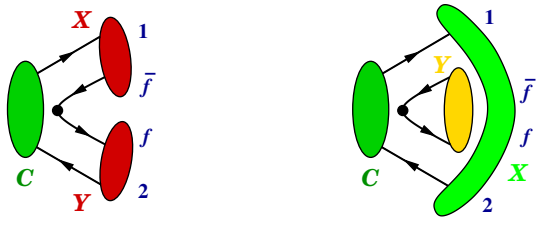

Fig. 2. Direct and crossed flavour arrangement and colour flow guaranteeing colour neutrality for each final-state configuration in cluster two-body decays

[6] For mesons this also includes the possibility of singlet–octet mixing occurring in hadron multiplets.

Table 1. Different cluster types emerging through cluster break-ups. Decay channels indicating a four-quark, i.e. two-diquark, system to become a hadron within the modes $\mathcal{C} \to \mathcal{C}_1\mathcal{H}_2$, $\mathcal{H}_1\mathcal{C}_2$, $\mathcal{H}_1\mathcal{H}_2$ are vetoed. The four-quark cluster disintegration into two mesons (see the last row of the table) is only available for the mode $\mathcal{C} \to \mathcal{H}_1\mathcal{H}_2$. The occurrence of the two disintegration possibilities is taken to be equally likely

Cluster		Direct case	Crossed case	Cluster		Direct case	Crossed case
$q_1\bar{q}_2$	$\xrightarrow{\bar{q}q}$	$q_1\bar{q} + q\bar{q}_2,$	$q_1\bar{q}_2 + q\bar{q}$	$q_1\bar{q}_2$	$\xrightarrow{D\overline{D}}$	$q_1 D + \overline{D}\bar{q}_2,$	$q_1\bar{q}_2 + \overline{D}D$
$q_1 D_2$	$\xrightarrow{\bar{q}q}$	$q_1\bar{q} + qD_2,$	$q_1 D_2 + q\bar{q}$	$q_1 D_2$	$\xrightarrow{D\overline{D}}$	$q_1 D + \overline{D}D_2,$	$q_1 D_2 + \overline{D}D$
$\overline{D}_1 D_2$	$\xrightarrow{\bar{q}q}$	$\overline{D}_1\bar{q} + qD_2,$	$\overline{D}_1 D_2 + q\bar{q}$	$\overline{D}_1 D_2$	$\xrightarrow{D\overline{D}}$	$\overline{D}_1 D + \overline{D}D_2,$	$\overline{D}_1 D_2 + \overline{D}D$
$\overline{D}_1 D_2$	$\longrightarrow$	$q_2\bar{q}_1 + q_2'\bar{q}_1'$		$\overline{D}_1 D_2$	$\longrightarrow$	$q_2\bar{q}_1' + q_2'\bar{q}_1$	

$$p_{1,2} \;=\; \left(1 - \frac{Q_0}{M_\mathcal{C}}\right) p^\mathcal{C}_{1,2}\,, \qquad p_{\bar{f},f} \;=\; \frac{Q_0}{M_\mathcal{C}}\, p^\mathcal{C}_{2,1}\,, \quad (11)$$

where f and $\bar{f}$ label the momenta of the newly created flavour pair. Hence, for the two cluster arrangements (see Fig. 2) the momenta are given by $P^\mathcal{X}_{\text{dir.}} = p_1 + p_{\bar{f}}$, $P^\mathcal{Y}_{\text{dir.}} = p_f + p_2$ in the direct, and $P^\mathcal{X}_{\text{cross.}} = p_1 + p_2$, $P^\mathcal{Y}_{\text{cross.}} = p_f + p_{\bar{f}}$ in the crossed case, respectively. The underlying algorithm, i.e. the mass-categorisation idea, for cluster decays implicates the demand that the calculation of the daughter-cluster momenta must not break down for any possible $M_\mathcal{C}$. To guarantee well-behaved four-momenta in this fission breaking, i.e. to have well-defined $Q_0/M_\mathcal{C}$ fractions with $Q_0 < M_\mathcal{C}$, our model uses a parametrisation of a running Q_0 increasing monotonously with $M_\mathcal{C}$. This running depending on two parameters, $\hat{Q}_0$ and $\hat{M}_0$, with the constraint $\hat{Q}_0 < \hat{M}_0$, can be formulated as

$$Q_0(M_\mathcal{C}) \;=\; \frac{\hat{Q}_0 \cdot M_\mathcal{C}}{\hat{M}_0 + M_\mathcal{C}} \;<\; M_\mathcal{C}\,. \quad (12)$$

The ansatz reflects that with increasing mother-cluster mass the momentum transfer in the fission is allowed to be higher. But it also fulfills the need for saturation for very massive clusters, since the dominant scale for hadronisation is the QCD scale Λ_{QCD}. From this consideration, the meaning of the two parameters can be found. $\hat{Q}_0$ gives an upper limit on the hadronisation-energy scale. Thus, it takes over the role of the original Q_0 fission constant of the Webber model [21]. The decline towards lower cluster masses can be controlled by the value given to $\hat{M}_0$. Ultimately, both parameters are major tuning parameters of our model, but they are quite natural in the sense that one knows the range of meaningful values, which can be given to them and which are of the order of hadronisation energies and peak masses of the cluster mass distribution for $\hat{Q}_0$ and $\hat{M}_0$, respectively.

Having fixed the primary kinematics, via (11), and the combination of flavours and momenta to the new clusters, their masses can be deduced from the squares of their total four-momenta. Then, as stated above, the different decay modes $\mathcal{C} \to \mathcal{C}_1\mathcal{C}_2$, $\mathcal{C}_1\mathcal{H}_2$, $\mathcal{H}_1\mathcal{C}_2$, $\mathcal{H}_1\mathcal{H}_2$ are distinguished according to the resulting masses of the daughter clusters. All possible decay channels within each mode are comprehensively summarised in Table 1.

(1) For the case of break-ups involving clusters only, i.e. for $\mathcal{C} \to \mathcal{C}_1\mathcal{C}_2$, nothing has to be done in addition.

(2) If one of the daughter clusters falls into the hadronic regime, i.e. for $\mathcal{C} \to \mathcal{C}_1\mathcal{H}_2$ and $\mathcal{C} \to \mathcal{H}_1\mathcal{C}_2$, a suitable hadron has to be selected such that the hadron will be lighter than the cluster. The selection procedure follows the one outlined above for the $\mathcal{C} \to \mathcal{H}$ transformation; the recoil is taken by the daughter system, which belongs to the cluster regime.

(3) If both new clusters fall into the hadron regime, i.e. for purely hadronic decays $\mathcal{C} \to \mathcal{H}_1\mathcal{H}_2$, more severe manipulations are applied. First of all, the newly created flavour pair $f\bar{f}$ is abandoned; instead, two hadrons are chosen directly. Then the combined weight for the selection of such a hadron pair consists of three pieces. The first part accounts for the two flavour-spin contents. The second one includes the correct relation of direct to crossed decay configurations and, furthermore, represents the incorporation of the pair-production rates. The last part considers the phase space of the decay, which is taken to be isotropic in the cluster's rest frame [19,21]. The combination of the first two weights for the hadron pair is set up as if only complete $\text{SU}(3)_F$ multiplets were accessible. Because of the superposition with the phase-space factor, a hadron pair that cannot be produced in a cluster decay owing to its large mass cannot contribute to the selection[7]. The other manipulation, as indicated above, is that once the hadron species are chosen, the cluster decays isotropically in its rest frame into these hadrons.

Two comments are in order here: first of all, our approach takes leading-particle effects into account in the same manner as in Webber's model [38]. This treatment on average enhances the anisotropy of leading-cluster break-ups. Secondly, when considering a cluster consisting of two diquarks, mesons can emerge only by recombining the individual quarks and antiquarks that constitute the diquarks; see Table 1. Since baryons appear in a decay of such clusters through the creation of a quark pair, the diquark recombination is taken to be suppressed by a factor of $p_\mathcal{B}$ with respect to the baryon production, which appears with $1 - p_\mathcal{B}$ in this channel. The specific ordering of the quarks into mesons is then done in a fashion similar to the one above, involving hadron pairs. The difference, however, lies

[7] The weight treatment for hadron selection in HERWIG was first modified by Kupčo [46]. However, recently, the HERWIG++ group has developed a new, improved, approach [16,26].

in the fact, that Clebsch–Gordan coefficients are additionally employed. These coefficients account for the rearrangement of the product of the diquark and antidiquark spin-S wave function into a double-mesonic basis, since after the break-up the (anti)diquark cannot be regarded as an entity anymore. The treatment, therefore, gives additional constraints on the spins of the emerging mesons. Given that these spins are denoted $S_{\mathcal{M}}$ and $S_{\mathcal{N}}$, one has to find the probabilities that their angular-momentum coupling results in the four-quark cluster's net spin, which is initially obtained from the spin coupling of its diquark and antidiquark. Using two-particle spin states $|SS_z\rangle_{12}$, the singlet and triplet vectors written in terms of single-particle spin functions are

$$\big|00\big\rangle_{12} = \frac{1}{\sqrt{2}}\Big(\big|\uparrow_1\downarrow_2\big\rangle - \big|\downarrow_1\uparrow_2\big\rangle\Big)\,, \tag{13}$$

$$\big|1\,{-1}\big\rangle_{12} = \big|\downarrow_1\downarrow_2\big\rangle\,, \tag{14}$$

$$\big|10\big\rangle_{12} = \frac{1}{\sqrt{2}}\Big(\big|\uparrow_1\downarrow_2\big\rangle + \big|\downarrow_1\uparrow_2\big\rangle\Big)\,, \tag{15}$$

$$\big|11\big\rangle_{12} = \big|\uparrow_1\uparrow_2\big\rangle. \tag{16}$$

Then, according to a $\overline{q_1q_2}q_3q_4$ cluster, for the $q_3\overline{q_1} + q_4\overline{q_2}$ combination, the, e.g. four-quark cluster spin-vector $|00\rangle_{12}|00\rangle_{34}$ formulated in terms of (anti)diquarks can be re-written as

$$\begin{aligned}\big|00\big\rangle_{12}\big|00\big\rangle_{34} = \frac{1}{2}\Big(&\big|11\big\rangle_{13}\big|1\,{-1}\big\rangle_{24} + \big|1\,{-1}\big\rangle_{13}\big|11\big\rangle_{24}\\ &-\big|10\big\rangle_{13}\big|10\big\rangle_{24} + \big|00\big\rangle_{13}\big|00\big\rangle_{24}\Big).\end{aligned} \tag{17}$$

This expression already allows one to read off the Clebsch–Gordan-like probabilities:

$$C_{00,00} = \frac{1}{4} \quad \text{and} \quad C_{00,11} = \frac{3}{4}\,, \tag{18}$$

where the notation $C_{S_{\overline{D}}S_D,S_{\mathcal{M}}S_{\mathcal{N}}}$ has been used. The other factors can be obtained in a similar fashion as illuminated above. One benefits from the fact that up to some change in signs the rearrangement for the other configuration $q_3\overline{q_2} + q_4\overline{q_1}$ yields the same results. Ultimately, one ends up with

$$C_{01,01} = C_{01,10} = \frac{1}{4} \quad \text{and} \quad C_{01,11} = \frac{1}{2}\,; \tag{19}$$

$$C_{10,01} = C_{10,10} = \frac{1}{4} \quad \text{and} \quad C_{10,11} = \frac{1}{2}\,; \tag{20}$$

$$C_{11,00} = \frac{1}{12}\,, \quad C_{11,01} = C_{11,10} = \frac{2}{12} \tag{21}$$

and

$$C_{11,11} = \frac{7}{12}\,. \tag{22}$$

5 Preliminary results

The performance of the model introduced above is now illustrated by presenting some results for e^+e^- annihilation at the Z^0-pole using only light quarks throughout the event's evolution. The outcomes have been obtained with the parton shower of APACIC++-1.0 [47], the matrix elements are generated by AMEGIC++-1.0 [48] and by using the CKKW approach [49] they are consistently matched with this parton shower, the primary hadronisation is accomplished by the cluster model described above, and the hadron decays are provided through interfacing the corresponding routines of PYTHIA-6.1 [6][8]. The resulting event generator is the combination of these modules. In the following it is referred to as SHERPAα. The results shown below were achieved with the same parameter set, where all cluster-model parameters were adjusted only manually by taking into account the full colour-reconnection model and by comparing against the corresponding PYTHIA-6.1 predictions. Table 2 summarises the major parameters of our cluster-hadronisation model, where the ones indicated by a star are referred to as the main tuning parameters of the model.

Table 2. Overview of the parameters and their values used in the cluster-hadronisation model of SHERPAα. Major tuning parameters are indicated through a star "$*$"

	Constituent masses		
	$M_{d,u}$	0.30	GeV
	M_s	0.45	GeV
	M_{ud_0}	0.57933	GeV
	M_{dd_1,ud_1,uu_1}	0.77133	GeV
	M_{sd_0,su_0}	0.80473	GeV
	M_{sd_1,su_1}	0.92953	GeV
	M_{ss_1}	1.09361	GeV
$*$	M_g	1.20	GeV
	Reconnection squared-mass scale		
	t_0	$1/4 \cdot M_g^2$	
	Strangeness production probability of pair creation		
$*$	p_s	0.104	
	Baryon production probability of pair creation		
$*$	$p_{\mathcal{B}}$	0.267	
	Relative orbital-angular-momentum weights		
	$\mathcal{P}_{L=0\ldots5},\ \mathcal{P}_{L>5}$	$1.5^{5-L},\ 0$	
	Cluster-fission mass scale of Q_0 running		
$*$	$\hat{Q}_0$	0.84	GeV
	Steepness regulator of Q_0 running		
$*$	$\hat{M}_0$	2.10	GeV
	Gaussian smearing parameter for leading-cluster break-ups $\mathcal{C}_\ell \to \mathcal{H}\mathcal{H}$		
$*$	σ_0	0.00077	

The settings of the other module's input variables were mainly taken over from a Z^0-pole tuning of APACIC++-1.0, together with the full hadronisation of PYTHIA-6.1, where the major modification amounted to a change of

[8] Although all complete SU(3)$_F$ hadron multiplets as given in the PDG Tables [50] have been implemented in our model, since invoking the PYTHIA-6.1 hadron decays for this first application, one has been restricted to only use the set of SU(3)$_F$ multiplets, which is identical to that one used by PYTHIA-6.1.

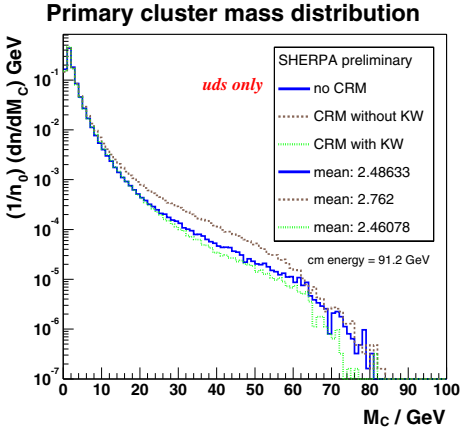

Fig. 3. Primary cluster-mass distribution in e^+e^- annihilation events that evolve into light-quark and gluon jets at the Z^0-pole. The SHERPAα results are shown for three cluster-model cases, the model excluding colour reconnection at all (solid line), the model using the kinematically unweighted colour reconnection, i.e. the colour-reconnection model (CRM) without kinematic weight (KW) (dashed line), and, the model including the full colour-reconnection treatment (dotted line)

the parton-shower cut-off, $t_{\rm cut}$, from $t_{\rm cut} = 0.5\,{\rm GeV}^2$ to $t_{\rm cut} = 0.4225\,{\rm GeV}^2$. Since measurements that specifically concentrate on the observation of light-quark characteristics are rarely available, our results are mainly compared with those gained from running PYTHIA-6.1 and HERWIG-6.1 [51] both restricted to u, d, s quarks. In doing so, either of the models has been run with its default parameter values.

In a first step internal model results are considered. To begin with, the effects of our colour-reconnection model on the cluster-mass distribution, and the statistics of the reconnections in the cluster formation are briefly discussed. Figure 3 illustrates the statement that under the influence of the kinematically re-weighted colour-reconnection model our cluster hadronisation tends to produce less massive primary clusters than without the full reconnection procedure.

This is in contrast to other colour-reconnection models. However, if one considers the kinematically unweighted model, which uses $w_{ij} \equiv 0$, the behaviour is completely reversed. Therewith one can conclude, first, that the decrease is especially caused by the kinematic factor, (1), where $w_{ij} = p_{\perp ij}$ has been used, and, second, that this factor has rather strong effects on the primary-cluster mass distribution. For the full (kinematically unweighted) colour-reconnection model in the cluster formation one gets approximately 0.742 (0.689) reconnections per event and, with a frequency of 47.7%, 35.2%, 13.0%, 3.3% (50.3%, 34.5%, 11.8%, 2.8%), and 0.8% (0.6%), one finds 0, 1, 2, 3, and > 3 exchange(s), respectively. Moreover, changing the option full colour reconnection while keeping the parameters (adjusted under the full reconnection model) unchanged yields the following qualitative modifications: for both other options, the number of daughter clusters per event is increased, which results for the reconnection-free and the kinematically unweighted model in an enlargement of the mean charged-particle multiplicity of roughly 0.2 and 1.0 charged tracks per event, respectively. In the free case the charged-pion production rate increases, where this is even more enhanced for the kinematically unweighted reconnection model. The charged-kaon rate and the (anti) proton rate decrease for the free model. These two effects are reversed for the reconnection model without kinematic weighting procedure. Furthermore, the charged-particle transverse-momentum distributions are lowered for high $p_\perp^{uds,{\rm in/out}}$, where the deviation is smaller for the model with the reconnection option entirely switched off. Again, this is an example where one may recognise a complete reverse of the full model's behaviour when the kinematic weighting procedure is not taken into account. In contrast, at the same time the scaled-momentum distribution of charged tracks alters only marginally. However, this is not true for the reconnection-free model. In this circumstance the scaled-momentum distribution's bump at $x_p^{uds} \approx 0.5$ is enhanced and the tail of the distribution tends to become harder (see the discussion below and cf. Fig. 8).

Briefly, the influence of exchanging the $p_{\perp ij}$ with the m_{ij} measure is discussed. In the multiplicity, event-shape, jet-rate and momentum distributions differences are barely noticeable. Modifications can only be reported from the primary-cluster mass distribution; see Fig. 4. There one may conclude that up to a small region around 10 GeV the m_{ij} model predicts a slightly harder spectrum; however, the

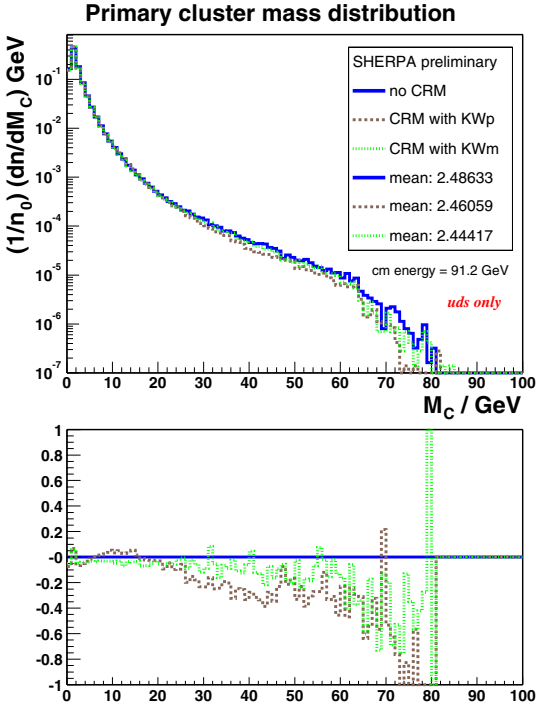

Fig. 4. Primary cluster-mass distribution in e^+e^- annihilation events that evolve into light-quark and gluon jets at the Z^0-pole. The SHERPAα results are shown for three cluster-model cases, the model excluding colour reconnection at all (solid line), the $p_{\perp ij}$ model (KWp) (dashed line), and, the m_{ij} model (KWm) (dotted line), both of which considering the complete treatment for colour reconnection. The lower part of the plot shows the normalised difference where the colour-reconnection free model is used as the reference

Table 3. Overall mean charged-particle multiplicity, and production rates of charged pions, charged kaons and (anti)protons in e^+e^- collisions. The values are taken for uds events running at the Z^0-peak centre-of-mass energy. The errors indicated in the table are the total errors of the measurements. More JETSET and HERWIG results on this topic can be found in [52]

	$\langle \mathcal{N}_{\rm ch}^{uds} \rangle$	$\langle \mathcal{N}_{\pi^\pm}^{uds} \rangle$	$\langle \mathcal{N}_{K^\pm}^{uds} \rangle$	$\langle \mathcal{N}_{p,\bar{p}}^{uds} \rangle$
PYTHIA-6.1(uds)	19.84	16.72	2.010	0.856
HERWIG-6.1(uds)	18.86	15.37	1.693	1.568
SHERPAα	20.15	16.83	2.018	1.047
OPAL [53]	20.25 ± 0.39			
DELPHI [54]	20.35 ± 0.19			
DELPHI [52]	19.94 ± 0.34	16.84 ± 0.87	2.02 ± 0.07	1.07 ± 0.05
SLD [55]	20.21 ± 0.24			
SLD [56]	20.048 ± 0.316	16.579 ± 0.304	2.000 ± 0.068	1.094 ± 0.043

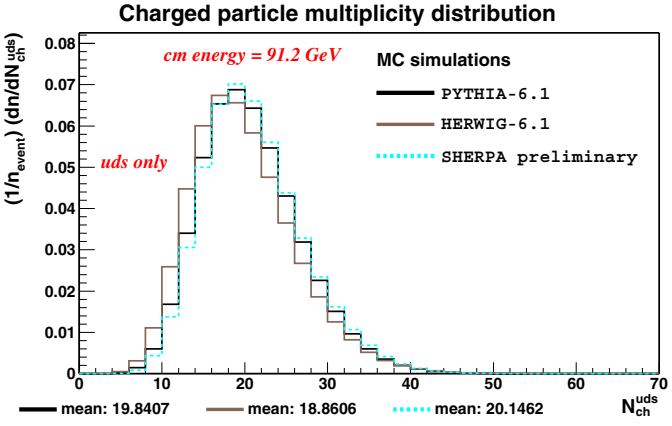

Fig. 5. Predicted multiplicity distribution of charged particles in e^+e^- annihilation for light-quark and gluon jets at the Z^0-pole. The SHERPAα result is shown together with the default PYTHIA-6.1(uds) and HERWIG-6.1(uds) predictions

trend given by the kinematical weighting is clearly retained. Also this does not seem to have great effects on hadron-level distributions, differences can also be seen in the statistics of the reconnections, since in the cluster formation now one gets approximately 0.564 reconnections per event and, with a frequency of 58.1%, 30.3%, 9.1%, 2.0%, and 0.5%, one finds 0, 1, 2, 3, and > 3 exchange(s), respectively. Hence, from the considerations done so far, one cannot judge which of the two measures is more suitable. In conclusion, the impact of the kinematical weighting has been clearly seen to be very crucial. So, to shed more light on the effects of the reconnection model, one has to explore observables that are specifically sensitive to colour reconnection. This then might favour the possibility of an isolated tuning of the kinematic factor, i.e. the choice of t_0 given in (1). Right now t_0 is set through 1/4 of the gluon constituent mass squared.

Now, in the second step, the preliminary predictions of our model under the inclusion of the full colour-reconnection model are discussed.

The overall charged-particle multiplicity distribution is presented in Fig. 5. The shift to higher multiplicities of the SHERPAα curve with respect to the other curves indicates the higher mean value of the SHERPAα prediction. Table 3 shows mean multiplicities $\langle \mathcal{N}_{\rm ch}^{uds} \rangle$ as provided by those three fragmentation models in comparison with inclusive measurements. To exemplify the charged-hadron rates, the mean multiplicities for the stable charged hadrons – $\pi^\pm$, $K^\pm$ and $p, \bar{p}$ – are considered and compared with experimental uds results; see also Table 3.

To have a comparison with experimental data on charged-particle multiplicity distributions, each event is divided into hemispheres using the plane perpendicular to the thrust axis. The charged-particle tracks per hemisphere are summed for both hemispheres. Then, the average of the two contributions is formed. This procedure yields the hemisphere multiplicity distribution of charged tracks, whereas the forward–backward asymmetry is not taken into account. The resulting SHERPAα distribution is shown in Fig. 6. There it is compared with experimental data from the OPAL collaboration [57].

In a further test the SHERPAα predictions for the energy dependence of the $\langle \mathcal{N}_{\rm ch} \rangle$ observable have been considered by using the Z^0-pole adjusted parameters. To do so, the corresponding $\langle \mathcal{N}_{\rm ch}^{uds} \rangle$ results have been corrected by employing an ansatz

$$\langle \mathcal{N}_{\rm ch} \rangle \;=\; \langle \mathcal{N}_{\rm ch}^{uds} \rangle \;+\; f_c\,\delta_c \;+\; f_b\,\delta_b\,, \qquad (23)$$

which has been quite similarly formulated in [58]. This ansatz exploits the QCD prediction that the difference in charged-particle multiplicity, $\delta_{c,b}$, between heavy- and light-quark events is expected to be almost energy independent [59]. The $f_{c,b}$ are the fractions of $c\bar{c}, b\bar{b}$ events, which can be obtained from APACIC++-1.0 when dropping the uds quark restriction[9]. To accomplish the calculation, a weighted average including results from low-energy data, LEP1 and LEP2, $\delta_b = 3.05 \pm 0.19$ [58], has been chosen; $\delta_c = 1.7 \pm 0.5$ has been taken from [59]. The resulting SHERPAα energy behaviour is shown in Fig. 7, where it is also compared with measurements from various e^+e^- experiments [50].

[9] In the calculation of the correction of the Monte Carlo result for 10 GeV, the b-quark threshold has been assumed to be above that energy, i.e. in this case f_b has been set to zero.

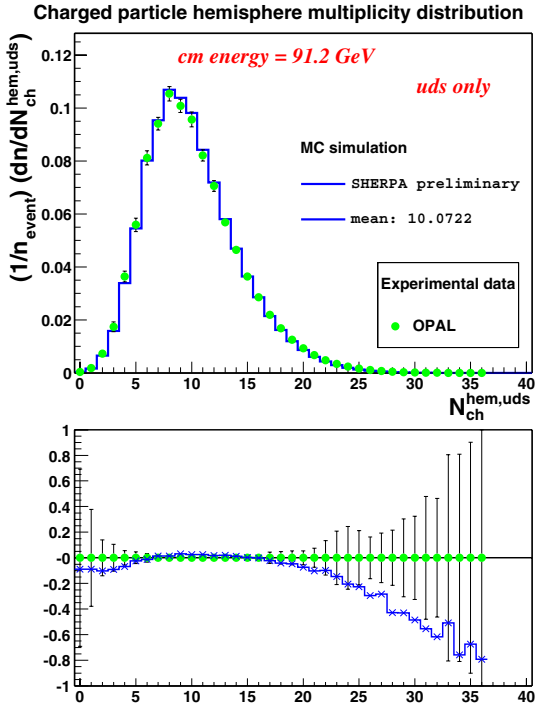

Fig. 6. Predicted hemisphere multiplicity distribution of charged tracks in electron–positron annihilation for the light-quark sector at the Z^0-pole. The hadron level prediction of SHERPAα is shown in comparison to the corrected distribution of charged-particle multiplicity obtained by OPAL [57]. The total uncertainties are indicated by vertical lines. The lower part of the plot illustrates the normalised difference between the simulation and the data

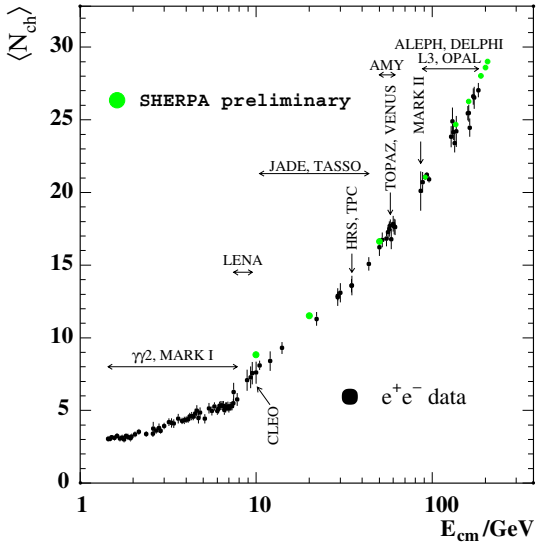

Fig. 7. Energy dependence of the mean charged-particle multiplicity in electron–positron annihilation. First predictions of SHERPAα employing a heavy-quark correction are shown in comparison to experimental e^+e^- data [50]. The total uncertainties of the measurements are indicated by vertical lines. The diameter of the SHERPAα points specifies the error due to the correction procedure

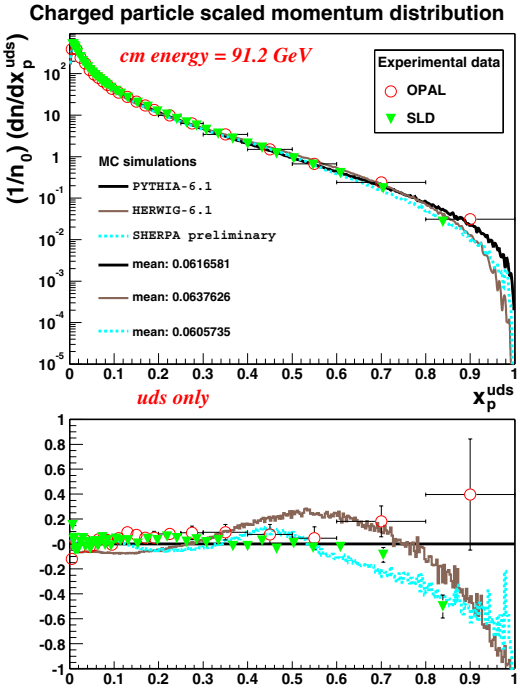

Fig. 8. Scaled momentum distribution of charged particles for $E_{\rm cm} = 91.2\,\text{GeV}$ in e^+e^- annihilation considering only the light-quark sector. The SHERPAα prediction is compared with experimental light-quark data provided by the OPAL [53] and SLD [56] collaborations. The total uncertainties are represented by vertical error bars, whereas the horizontal lines attached to the OPAL data points indicate the x_p^{uds} range for the corresponding measurement. Also shown are the outcomes of PYTHIA-6.1(uds) and HERWIG-6.1(uds) in their default settings. Concerning the mean value $\langle x_p^{uds} \rangle$ of the distributions, only the HERWIG-6.1(uds) prediction is consistent with the OPAL measurement of $\langle x_p^{uds} \rangle = 0.0630 \pm 0.0003$ (stat.) $\pm$ 0.0011 (syst.) [53]. As before, the lower part of the plot represents the normalised difference, however, the PYTHIA-6.1(uds) prediction is now used as the reference curve

In view of all these multiplicity comparisons, one can conclude that the obtained SHERPAα multiplicity results are in reasonable agreement with the PYTHIA-6.1(uds) predictions and with the data.

As an example for a particle-momentum distribution the scaled momentum $x_p^{uds} = 2|\mathbf{p}_{uds}|/E_{\rm cm}$ and its negative logarithm $\xi_p^{uds} = -\ln x_p^{uds}$ are considered. The x_p^{uds} distribution obtained with SHERPAα is shown in Fig. 8, together with the predictions of the PYTHIA-6.1(uds) and HERWIG-6.1(uds) event generators. Furthermore, experimental results delivered by the OPAL [53] and SLD [56] collaborations on this differential cross section have been included. Additionally, in Fig. 9 DELPHI data [52] are compared with the predictions of the fragmentation models under consideration. In order to enhance the significance, a histogram structure being identical to that one of the data has been used for the calculation of the simulated x_p^{uds} values. The PYTHIA-6.1(uds) model is the most consistent with the OPAL and DELPHI data, but it predicts a slightly softer spectrum. Both cluster-hadronisation models show quite similar behaviour concerning their devia-

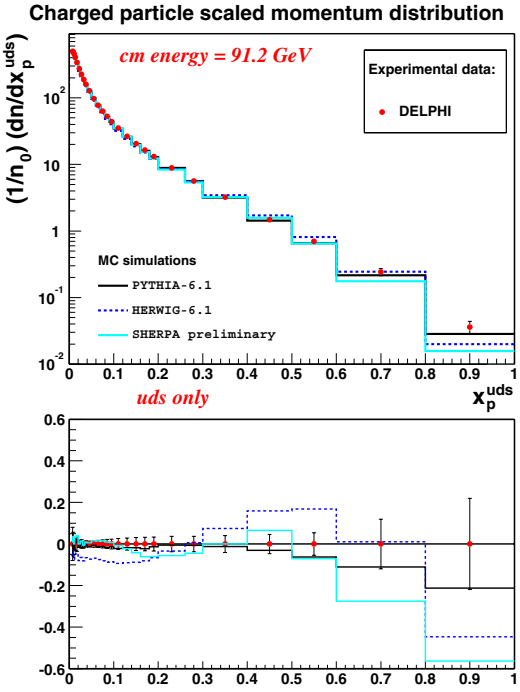

Fig. 9. Scaled momentum distribution of charged particles for $E_{\rm cm} = 91.2\,\text{GeV}$ in electron–positron annihilation considering only the light-quark sector. The SHERPAα prediction is compared with experimental light-quark data provided by the DELPHI collaboration [52]. The total uncertainties are shown by vertical lines. Also included are the predictions of default PYTHIA-6.1(uds) and default HERWIG-6.1(uds). The lower part of the plot represents the normalised difference between the Monte Carlo models and the data

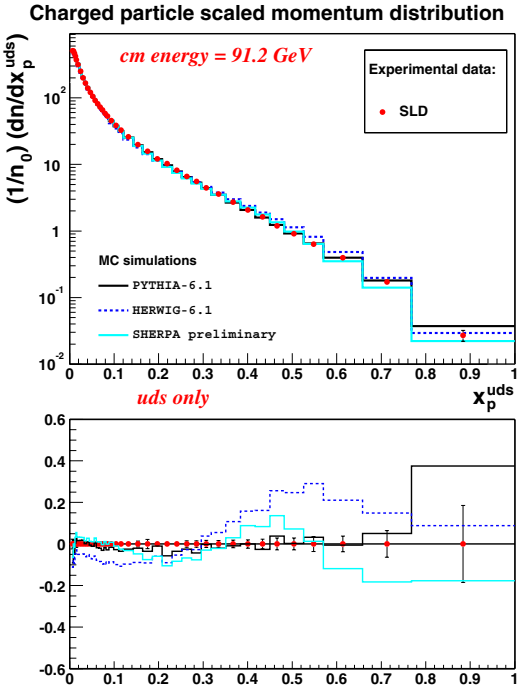

Fig. 10. Scaled momentum distribution of charged particles for $E_{\rm cm} = 91.2\,\text{GeV}$ in electron–positron annihilation considering only the light-quark sector. The SHERPAα prediction is compared with experimental light-quark data provided by the SLD collaboration [56]. The total uncertainties are shown by vertical lines. Also included are the predictions of default PYTHIA-6.1(uds) and default HERWIG-6.1(uds). The lower part of the plot again represents the normalised difference between the Monte Carlo models and the data

tion from the PYTHIA-6.1(uds) prediction (cf. Fig. 8). For $x_p^{uds} < 0.7$ they oscillate around this prediction, where both have the tendency to overestimate the data at $x_p^{uds} \approx 0.5$. For $x_p^{uds} > 0.75$ they anticipate a steeper decline, which is quite different from that seen in the OPAL and DELPHI data. In spite of these shortcomings, the agreement of SHERPAα with the DELPHI data is encouraging at least up to x_p^{uds} values of 0.6 (cf. Fig. 9). Moreover, the recently published SLD results [56] already plotted in Fig. 8 show a considerably softer high-x_p^{uds} tail. To better judge the performance of our model according to the SLD data, again a histogram structure being identical to the data binning has been used; see Fig. 10. The soft high-x_p^{uds} tail behaviour then can be described by our cluster model and by the HERWIG model as well, which is above our prediction. Nevertheless, in our case the onset of the rapid fall off is still at scaled-momentum values that are too low. When going towards lower x_p^{uds}, the first bump is truly a deficiency of cluster approaches. In comparison with the HERWIG-6.1(uds) prediction (see Figs. 9 and 10), our model yields, however, a smaller bump, and the values for $x_p^{uds} > 0.7$ show a softer decline, i.e. do not fall off as rapidly as the HERWIG-6.1(uds) ones[10]. This slightly better performance might be gained due to the mass-categorisation treatment of the cluster transitions which has been introduced in our model.

All in all, our x_p^{uds} behaviour clearly reflects two symptomatic cluster-model weaknesses, namely
(1) that the necessary increase in cluster and, therefore, in hadron multiplicity excessively results in a decrease of large three-momenta of primary clusters, and
(2) that the hadronisation of events with a small number of primary clusters is not sufficiently modelled yet. Both statements can be seized more properly. In the first case this behaviour does not necessarily have to be wrong, but, surely, one has to carefully tune, in interplay with the overall mean charged-particle multiplicity, the decline towards higher x_p^{uds}. But, unfortunately, there is not only this enhanced decline. Truly a weak point of the cluster model is the formation of bumps in the x_p^{uds} distribution. This is a sign that the underlying fission kinematics is still not sufficiently adapted to the needs of hadronisation, at least when considering the light-quark sector only. To support this statement two different scenarios have been compared and the x_p^{uds} distribution is plotted in Fig. 11 with the reference curve obtained from PYTHIA-6.1(uds). The pure case of allowing only $\mathcal{C} \to \mathcal{H}_1\mathcal{H}_2$ break-ups has been tested

[10] Contrary to the old FORTRAN HERWIG, recently published HERWIG++-1.0 results on the topic show an improved behaviour, which is different to that one of FORTRAN HERWIG-6.1(uds) [16].

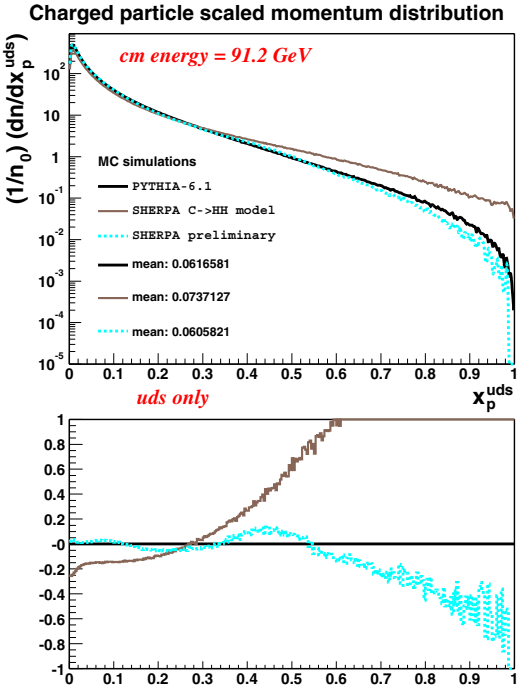

Fig. 11. Scaled momentum distribution of charged particles for $E_{\mathrm{cm}} = 91.2\,\mathrm{GeV}$ in electron–positron annihilation considering only the light-quark sector. The SHERPAα prediction is compared with the SHERPAα $\mathcal{C} \to \mathcal{H}\mathcal{H}$ model prediction. As the reference curve the result of default PYTHIA-6.1(uds) is included. Then, the lower part of the plot represents the normalised difference between the PYTHIA-6.1(uds) model and the SHERPAα models

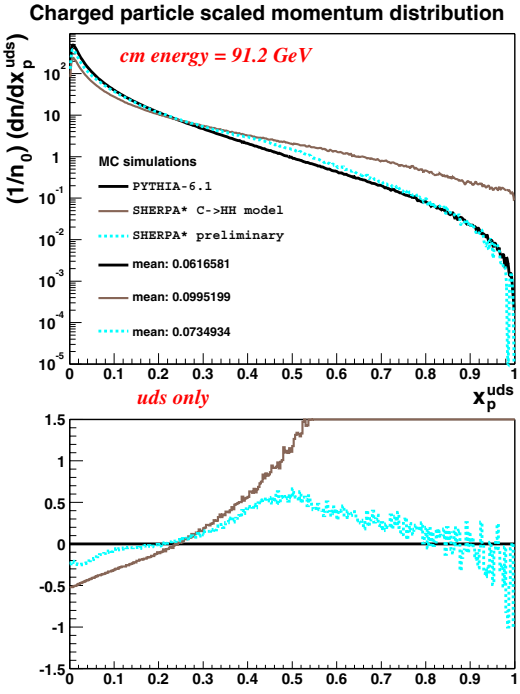

Fig. 12. Scaled momentum distribution of charged particles for $E_{\mathrm{cm}} = 91.2\,\mathrm{GeV}$ in electron–positron annihilation considering only the light-quark sector. The SHERPA$\alpha*$ prediction is compared with the SHERPA$\alpha*$ $\mathcal{C} \to \mathcal{H}\mathcal{H}$ model prediction. The star indicates that, for this analysis, only events with a primary-cluster number lower than 7 have been taken into account. The reference curve is given by the default PYTHIA-6.1(uds) outcome. So, the lower part of the plot represents the normalised difference between the PYTHIA-6.1(uds) model and the SHERPA$\alpha*$ models

against the full SHERPAα model. One gets exactly the expected behaviour; the $\mathcal{C} \to \mathcal{H}_1\mathcal{H}_2$ model is much lower in multiplicity and shows a harder high-x_p^{uds} tail. But up to a small bump at very high x_p^{uds}, its corresponding distribution is free of bumps. This may lead to the conclusion that all the change in the scaled-momentum distribution comes from the cluster-decay kinematics, cf. (11). Moreover, the formation of the hadron-level bumps may be explained as follows. In our case of light quarks the leading term for the daughter-cluster masses is the same, $M^2_{\mathcal{X},Y} \sim Q_0 M_{\mathcal{C}} - Q_0^2$. This then is an advantage for the emergence of quite symmetrical mass configurations for the decay products and, in turn, the $\mathcal{C} \to \mathcal{C}_1\mathcal{C}_2$ and $\mathcal{C} \to \mathcal{H}_1\mathcal{H}_2$ break-ups will appear very often. This furthermore translates into the effects that, firstly, scaled-momentum ranges emerge where the kinematics prefers to place the new momenta and, secondly, regions arise where non-purely hadronic decays are very suppressed and therefore the x_p^{uds} behaviour tries to follow the one of the $\mathcal{C} \to \mathcal{H}_1\mathcal{H}_2$ model. This is quite adequately illustrated in Fig. 12 where, for the SHERPAα model, events with a primary-cluster multiplicity lower than 7 have been explicitly considered[11]. The outcome of this plot clearly puts emphasis on the second statement that especially for events with a low multiplicity in primary clusters the cluster hadronisation is still problematic. Taken together, the main problem is the somewhat deficient interplay of the cluster-decay kinematics with the purely isotropic one taken to manage the $\mathcal{C} \to \mathcal{H}_1\mathcal{H}_2$ transitions. The "decline problem" can be concluded to manifest itself as a problem which may be tuned away through carefully tuning the perturbative and non-perturbative parameters simultaneously, whereas the "bump problem" implies one should introduce corrections to the cluster-decay kinematics.

In contrast to the x_p^{uds} distribution, the ξ_p^{uds} distribution emphasises the soft momenta of the spectrum. Figure 13 illuminates the SHERPAα result together with those of the other two QCD Monte Carlo models and compares them with experimental measurements from the OPAL collaboration [53]. PYTHIA-6.1(uds) describes the data over the full ξ_p^{uds} region. Except for the first three data points (the region of hard momenta), SHERPAα can also reasonably describe the data and is comparable to the PYTHIA-6.1(uds) prediction. It slightly underestimates the region of $1.0 < \xi_p^{uds} < 2.0$. HERWIG-6.1(uds) is low (high) for $2.0 < \xi_p^{uds} < 5.0$ ($0.4 < \xi_p^{uds} < 1.0$). The outcomes of the three Monte Carlo simulations all reproduce a peak position of $\xi_{p,\mathrm{MC}}^{*,uds} = 3.7 \pm 0.1$, which reasonably coincides with the experimental inclusive measurements of

[11] This coincides with the peak position of the primary-cluster multiplicity distribution.

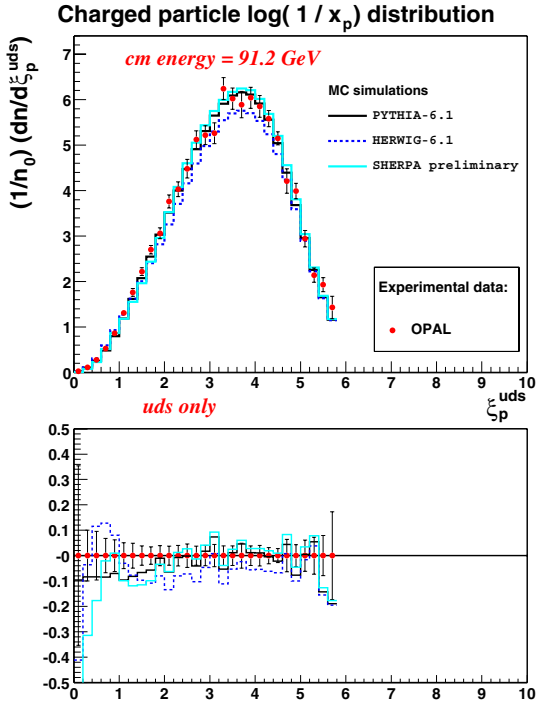

Fig. 13. $\xi_p^{uds} = \ln(1/x_p^{uds})$ distribution of charged particles for $E_{\rm cm} = 91.2\,\text{GeV}$ in electron–positron annihilation, considering the light-quark sector only. The SHERPAα prediction is presented together with experimental uds data provided by the OPAL collaboration [53], and with results from default PYTHIA-6.1(uds) and default HERWIG-6.1(uds). The total uncertainties are shown by vertical error bars. The lower part of the plot visualises the normalised difference between the Monte Carlo simulations and the data

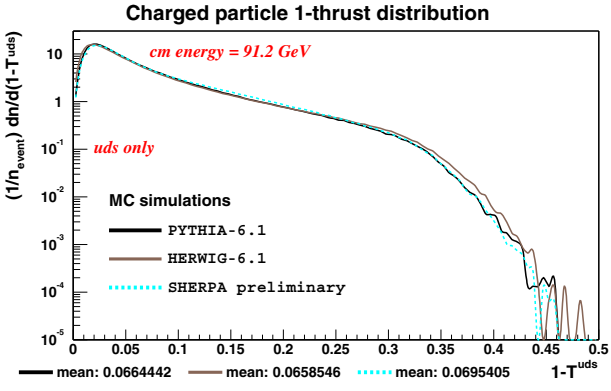

Fig. 14. $1 - T^{uds}$ distribution of charged particles for $E_{\rm cm} = 91.2\,\text{GeV}$ in e^+e^- annihilation with a restriction on u, d, s and gluon jets. The SHERPAα prediction is compared with predictions of default PYTHIA-6.1(uds) and HERWIG-6.1(uds)

the peak position, $\xi_p^{*,uds} = 3.76 \pm 0.02$ (DELPHI [52]) and $\xi_p^{*,uds} = 3.74 \pm 0.22$ (OPAL [53]).

As an example for the group of event-shape observables, the $1 - T^{uds}$ distribution – with T^{uds} being the thrust – of the three aforementioned QCD Monte Carlo event generators with u, d, s quark restriction is presented in Fig. 14 for light-quark and gluon jets. HERWIG-6.1(uds) accounts

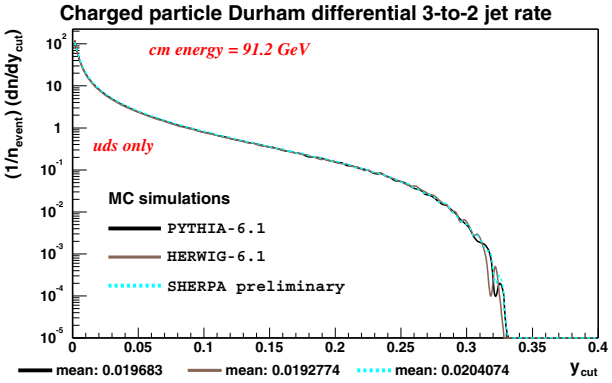

Fig. 15. The Durham $3 \to 2$ differential jet rate of charged particles in electron–positron annihilation at the Z^0-pole. Only uds events are taken into account. The SHERPAα result is compared with the results stemming from PYTHIA-6.1(uds) and HERWIG-6.1(uds) performances, both of which run with their default parameters

on average for more spherical event shapes, which is indicated by a softer decline of the spectrum towards higher values. The SHERPAα prediction, somewhat exceeding the PYTHIA-6.1(uds) result for $0.1 < 1 - T^{uds} < 0.3$, rather resembles the prediction of PYTHIA-6.1(uds), which, owing to the LPHD concept, might be due to the fact that SHERPAα employs a PYTHIA-like parton shower.

Lastly the Durham $3 \to 2$ differential jet rate is considered in Fig. 15. Except for the low-statistics region, the results for the event generators shown in the plot barely exhibit any deviation from one another.

Taken together, the first experiences with the performance of SHERPAα are promising. Reasonable agreement could be achieved in comparisons with PYTHIA-6.1 restricted onto the light-quark sector and, where provided, with experimental data for electron–positron annihilation into light-quark and gluon jets at the Z^0-pole. The model has not been extensively tuned yet, i.e. the new model's parameters have not been fitted to the data yet.

6 Summary and conclusions

A modified cluster-hadronisation model has been presented. In comparison with the long-standing Webber model, the extensions of our approach are the following.

Soft colour-reconnection effects are included in the cluster-formation as well as in the cluster-decay processes. This yields an enhancement of the number of decay configurations. The spin of diquarks is explicitly accounted for throughout the model. The number of basic cluster species is enlarged, especially by a new mesonic-cluster type, the four-quark cluster. The significant feature of our approach is the flavour-dependent separation of the cluster and hadron regimes in terms of the mother cluster's mass. This categorisation automatically selects the cluster-transition mode. Taken together, these aspects require the set-up of generically new cluster-decay channels.

Our cluster-hadronisation model is implemented as a C++ code. The resulting version is capable of describing electron–positron annihilation $e^+e^- \to \gamma^*/Z^0 \to d\bar{d}, u\bar{u}, s\bar{s}$ into light-quark and gluon jets. Some first tests were passed (see previous section) and the agreement with PYTHIA-6.1(uds) and experimental data is satisfactory. Some cluster-model shortcomings, such as the too low charged-particle multiplicity, could be cured; and the spectrum of the scaled momentum could be improved. The model will soon be completed by including heavy-quark hadronisation. Furthermore, the focus of future work is on treating the fragmentation of remnants of incoming hadrons, especially in view of proton–(anti)proton applications (Tevatron and LHC physics) [60].

Acknowledgements. J.W. and F.K. would like to thank Bryan Webber, Torbjörn Sjöstrand, Rick Field, Leif Lönnblad, Stefan Gieseke, Philip Stevens, Alberto Ribon and Mike Seymour for fruitful and pleasant communication on the subject.

J.W. and F.K. are indebted to Klaus Hamacher and Hendrik Hoeth for valuable discussions, especially on the outcome of the model.

Special thanks go to Suzy Vascotto for carefully reading the manuscript.

J.W. would like to thank the TH division at CERN for kind hospitality during the MC4LHC workshop, where parts of this work were completed.

F.K. acknowledges financial support from the EC 5th Framework Programme under contract number HPMF–CT–2002-01663. The authors are grateful for additional financial support by GSI, BMBF and DFG.

References

1. Y.L. Dokshitzer, V.A. Khoze, A.H. Mueller, S.I. Troian, Basics of perturbative QCD (Editions Frontières, Gif-sur-Yvette 1991)
2. R.K. Ellis, W.J. Stirling, B.R. Webber, QCD and Collider Physics, Cambridge Monogr. Part. Phys. Nucl. Phys. Cosmol. **8**, 1 (1996)
3. B. Andersson, The Lund Model, Cambridge Monogr. Part. Phys. Nucl. Phys. Cosmol. **7**, 1 (1997)
4. G. Gustafson, Phys. Lett. B **175**, 453 (1986); G. Gustafson, U. Pettersson, Nucl. Phys. B **306**, 746 (1988); B. Andersson, G. Gustafson, L. Lönnblad, Nucl. Phys. B **339**, 393 (1990)
5. L. Lönnblad, Comput. Phys. Commun. **71**, 15 (1992)
6. T. Sjöstrand, P. Eden, C. Friberg, L. Lönnblad, G. Miu, S. Mrenna, E. Norrbin, Comput. Phys. Commun. **135**, 238 (2001) [hep-ph/0010017]
7. T. Sjöstrand, L. Lönnblad, S. Mrenna, hep-ph/0108264; T. Sjöstrand, L. Lönnblad, S. Mrenna, P. Skands, hep-ph/0308153
8. G. Corcella et al., JHEP **0101**, 010 (2001) [hep-ph/0011363]
9. G. Corcella et al., hep-ph/0210213
10. R.D. Field, R.P. Feynman, Nucl. Phys. B **136**, 1 (1978); Phys. Rev. D **15**, 2590 (1977)
11. X. Artru, G. Mennessier, Nucl. Phys. B **70**, 93 (1974); M.G. Bowler, Z. Phys. C **11**, 169 (1981)
12. B. Andersson, G. Gustafson, B. Söderberg, Z. Phys. C **20**, 317 (1983); Nucl. Phys. B **264**, 29 (1986)
13. B. Andersson, G. Gustafson, G. Ingelman, T. Sjöstrand, Phys. Rep. **97**, 31 (1983)
14. T. Sjöstrand, Phys. Lett. B **142**, 420 (1984); Nucl. Phys. B **248**, 469 (1984)
15. C.D. Buchanan, S.B. Chun, Phys. Rev. Lett. **59**, 1997 (1987); S.B. Chun, C.D. Buchanan, Phys. Lett. B **308**, 153 (1993); Phys. Rep. **292**, 239 (1998)
16. S. Gieseke, A. Ribon, M.H. Seymour, P. Stephens, B. Webber, JHEP **0402**, 005 (2004) [hep-ph/0311208]
17. K. Odagiri, JHEP **0307**, 022 (2003) [hep-ph/0307026]; I. Borozan, M.H. Seymour, JHEP **0209**, 015 (2002) [hep-ph/0207283]; P. Richardson, JHEP **0111**, 029 (2001) [hep-ph/0110108]; F.M. Liu, H.J. Drescher, S. Ostapchenko, T. Pierog, K. Werner, J. Phys. G **28**, 2597 (2002) [hep-ph/0109104]; T. Sjöstrand, O. Smirnova, C. Zacharatou Jarlskog, Eur. Phys. J. C **21**, 93 (2001) [hep-ph/0104118]; V. Berezinsky, M. Kachelriess, Phys. Rev. D **63**, 034007 (2001) [hep-ph/0009053]; H.J. Drescher, M. Hladik, S. Ostapchenko, T. Pierog, K. Werner, Phys. Rep. **350**, 93 (2001) [hep-ph/0007198]; Q. Wang, G. Gustafson, Q. b. Xie, Phys. Rev. D **62**, 054004 (2000) [hep-ph/9912310]
18. S. Wolfram, CALT-68-778, Largely based on a talk given at 15th Rencontre de Moriond, Les Arcs, France, March 9–21, 1980
19. R.D. Field, S. Wolfram, Nucl. Phys. B **213**, 65 (1983)
20. T.D. Gottschalk, Nucl. Phys. B **214**, 201 (1983); B **239**, 349 (1984); T.D. Gottschalk, D.A. Morris, Nucl. Phys. B **288**, 729 (1987)
21. B.R. Webber, Nucl. Phys. B **238**, 492 (1984)
22. G. Marchesini, B.R. Webber, Nucl. Phys. B **238**, 1 (1984); B **310**, 461 (1988)
23. B.R. Webber, in Proceedings of the 19th International Symposion on Photon and Lepton Interactions at High Energy, LP99, edited by J.A. Jaros, M.E. Peskin, Int. J. Mod. Phys. A **15S1**, 577 (2000) [eConf C990809 577 (2000)] [hep-ph/9912292]
24. D. Amati, G. Veneziano, Phys. Lett. B **83**, 87 (1979); A. Bassetto, M. Ciafaloni, G. Marchesini, Phys. Lett. B **83**, 207 (1979); G. Marchesini, L. Trentadue, G. Veneziano, Nucl. Phys. B **181**, 335 (1981)
25. Y.I. Azimov, Y.L. Dokshitzer, V.A. Khoze, S.I. Troian, Z. Phys. C **27**, 65 (1985)
26. See the presentations and the talks given at the MC4LHC Workshop at CERN, Geneva, Switzerland, July 7–August 1, 2003, http://mlm.home.cern.ch/mlm/mcwshop03/mcwshop.html
27. M. Bertini, L. Lönnblad, T. Sjöstrand, Comput. Phys. Commun. **134**, 365 (2001) [hep-ph/0006152]
28. L. Lönnblad, T. Sjöstrand, http://www.thep.lu.se/~leif/Pythia7/Welcome.html
29. S. Gieseke, hep-ph/0210294
30. S. Gieseke, A. Ribon, M. Seymour, P. Stephens, B.R. Webber, http://www.hep.phy.cam.ac.uk/~gieseke/Herwig++/
31. T. Gleisberg, S. Höche, F. Krauss, A. Schälicke, S. Schumann, J. Winter, JHEP **0402**, 056 (2004) [hep-ph/0311263]
32. A. Schälicke, T. Gleisberg, S. Höche, S. Schumann, J. Winter, F. Krauss, G. Soff, hep-ph/0311270
33. T. Gleisberg, S. Höche, F. Krauss, A. Schälicke, S. Schumann, J. Winter, http://www.physik.tu-dresden.de/~krauss/hep/

34. V.A. Khoze, W. Ochs, J. Wosiek, hep-ph/0009298, and references therein; Y.L. Dokshitzer, V.A. Khoze, S.I. Troian, Adv. Ser. Direct. High Energy Phys. **5**, 241 (1988)
35. G.C. Fox, S. Wolfram, Nucl. Phys. B **168**, 285 (1980); T. Sjöstrand, Phys. Lett. B **157**, 321 (1985)
36. P. Abreu et al. [DELPHI Collaboration], Z. Phys. C **73**, 11 (1996)
37. K. Hamacher, M. Weierstall, hep-ex/9511011
38. G. Corcella et al., http://www.hep.phy.cam.ac.uk/˜richardn/HERWIG/herwig65/manual.html
39. T. Sjöstrand, V.A. Khoze, Z. Phys. C **62**, 281 (1994) [hep-ph/9310242]
40. B.R. Webber, J. Phys. G **24**, 287 (1998) [hep-ph/9708463]
41. L. Lönnblad, Z. Phys. C **70**, 107 (1996)
42. J. Rathsman, Phys. Lett. B **452**, 364 (1999) [hep-ph/9812423]
43. A. Edin, G. Ingelman, J. Rathsman, Phys. Lett. B **366**, 371 (1996) [hep-ph/9508386]; Z. Phys. C **75**, 57 (1997) [hep-ph/9605281]; G. Ingelman, A. Edin, R. Enberg, J. Rathsman, N. Timneanu, Nucl. Phys. Proc. Suppl. B **79**, 386 (1999) [hep-ph/9912535]; R. Enberg, G. Ingelman, A. Kissavos, N. Timneanu, Phys. Rev. Lett. **89**, 081801 (2002) [hep-ph/0203267]
44. S. Catani, Y.L. Dokshitzer, M. Olsson, G. Turnock, B.R. Webber, Phys. Lett. B **269**, 432 (1991)
45. B. Andersson, G. Gustafson, T. Sjöstrand, Nucl. Phys. B **197**, 45 (1982); Phys. Scripta **32**, 574 (1985)
46. A. Kupčo, hep-ph/9906412
47. R. Kuhn, F. Krauss, B. Ivanyi, G. Soff, Comput. Phys. Commun. **134**, 223 (2001) [hep-ph/0004270]
48. F. Krauss, R. Kuhn, G. Soff, JHEP **0202**, 044 (2002) [hep-ph/0109036]
49. S. Catani, F. Krauss, R. Kuhn, B.R. Webber, JHEP **0111**, 063 (2001) [hep-ph/0109231]
50. K. Hagiwara et al. [Particle Data Group Collaboration], Phys. Rev. D **66**, 010001 (2002)
51. G. Corcella et al., hep-ph/9912396
52. P. Abreu et al. [DELPHI Collaboration], Eur. Phys. J. C **5**, 585 (1998)
53. K. Ackerstaff et al. [OPAL Collaboration], Eur. Phys. J. C **7**, 369 (1999) [hep-ex/9807004]
54. P. Abreu et al. [DELPHI Collaboration], Eur. Phys. J. C **6**, 19 (1999)
55. K. Abe et al. [SLD Collaboration], Phys. Lett. B **386**, 475 (1996) [hep-ex/9608008]
56. K. Abe et al. [SLD Collaboration], hep-ex/0310017
57. K. Ackerstaff et al. [OPAL Collaboration], Eur. Phys. J. C **1**, 479 (1998) [hep-ex/9708029]
58. G. Abbiendi et al. [OPAL Collaboration], Phys. Lett. B **550**, 33 (2002) [hep-ex/0211007]
59. B.A. Schumm, Y.L. Dokshitzer, V.A. Khoze, D.S. Koetke, Phys. Rev. Lett. **69**, 3025 (1992)
60. M.L. Mangano, hep-ph/0312117